The influence of walls on Lagrangian statistics in two-dimensional turbulence

B. Kadoch,[1] W. J. T. Bos,[2] and K. Schneider[1]
[1]*M2P2–CNRS & CMI, Aix–Marseille Université & Ecole Centrale Marseille, Marseille, France*
[2]*LMFA–UMR 5509 CNRS, Ecole Centrale de Lyon, Université de Lyon, Ecully, France*

(Received 1 March 2011; accepted 5 July 2011; published online 24 August 2011)

The influence of solid walls on the Lagrangian statistics of statistically stationary two-dimensional turbulence is investigated by comparing the flow in a circular wall-bounded and in an unbounded periodic domain. A Fourier pseudo-spectral method is used, which is combined in the wall bounded case with a volume penalization technique to impose no-slip conditions. A particular emphasis is put on the acceleration of fluid particles. It is investigated to what extent the impact of the boundaries influences the shape of the probability density functions of Lagrangian velocity increments. It is shown that the influence of walls is not confined to a small near-wall region but alters the statistics in the entire flow domain. This can be explained by the vorticity generation in the turbulent boundary layer which destabilizes and leads to the formation of vortices that subsequently detach and travel into the bulk flow. The enstrophy level is thus increased with respect to the one in the unbounded periodic domain. © *2011 American Institute of Physics*. [doi:10.1063/1.3623273]

I. INTRODUCTION

The small scale universality of high Reynolds number turbulence is a cornerstone of a large number of theories and engineering models.[1] Even though at a crude level this universality approximately holds since the energy cascade tends to gradually erase the large-scale anisotropy and inhomogeneity of turbulent flows, it becomes increasingly clear that fine statistics carry almost always a footprint of the non-universal large scales, see e.g., Ref. 2. This observation holds not only for Eulerian statistics but seems also to be true for Lagrangian fine-scale statistics. The study of the latter has known a revival of interest by the use of direct numerical simulation (DNS)[3] and more recently, new experimental techniques.[4,5] For a review on Lagrangian studies in three-dimensional turbulence, the reader is referred to Refs. 6 and 7. Studies on the Lagrangian statistics in two-dimensional turbulence are reported in Refs. 8–11. In particular, the fluid particle acceleration has received a tremendous amount of attention. Indeed, whereas the velocity (both in the Eulerian and Lagrangian framework) displays near Gaussian statistics, the Lagrangian acceleration shows a more intermittent behavior than the velocity, reflected by heavy tails in the probability density functions (PDFs). Even though the results of different numerical and physical experiments show common features, closer inspection shows small but significant differences between the PDFs for the Lagrangian acceleration, possible stemming from the flow geometry.[12–15] A first study assessing the influence of walls on Lagrangian statistics was recently carried out in the framework of two-dimensional turbulence.[16] In this work, a freely decaying two-dimensional flow in a double-periodic domain was compared to a flow bounded by circular walls. Clear differences were found between the two cases, in particular with respect to the PDF of the Lagrangian acceleration. The interpretation of the results was however non-trivial, since the energy-decay of the flow is accelerated in wall-bounded flows through the vorticity generation at the walls leading to increased dissipation.[17] In order to obtain converged PDFs in Ref. 16, quantities were averaged over a long time-interval, in which the influence of the energy decay was compensated by normalizing the velocity by the global root mean square velocity. This approach improves the convergence of the statistics but makes the comparison of the statistics between the two types of flows questionable. This motivates to carry out a study in which the turbulence is kept statistically stationary by injecting energy in the large flow scales. This is the main objective of the present study: completing and reassessing the results obtained in Ref. 16, but in the case of a statistically stationary flow.

The remainder of the paper is organized as follows. In Sec. II, we will describe the numerical method and the physical parameters which characterize the different flows. Then, in Sec. III, we will study the Lagrangian statistics. This section is decomposed into three parts: in the first part, we will characterize the effects of no-slip boundary conditions onto Lagrangian statistics; the second part will focus on the question if this influence is confined to a region of the flow or that it influences the complete flow; and in the third part, we assess the influence of the level of enstrophy on the standard deviation of the Lagrangian acceleration. Finally, several conclusions and perspectives are given.

II. NUMERICAL METHOD AND PHYSICAL PARAMETERS

In order to assess the influence of solid walls on the Lagrangian flow statistics, we consider two distinct geometries in this study: a square domain with periodic boundary conditions and a circular domain with no-slip boundary conditions. Two-dimensional incompressible turbulent flow with unit density is considered, governed by the Navier-Stokes

equations written in dimensionless form in vorticity-velocity formulation

$$\frac{\partial \omega}{\partial t} + \boldsymbol{u} \cdot \nabla \omega - \nu \nabla^2 \omega - \nabla \times \boldsymbol{F} = -\frac{1}{\eta} \nabla \times (\chi \boldsymbol{u}), \qquad (1)$$

where $\boldsymbol{u} = (u_1, u_2)$ is the velocity, $\omega = \nabla \times \boldsymbol{u}$ is the vorticity, ν is the kinematic viscosity, and $\boldsymbol{F}$ is an external force. The velocity field is assumed to be incompressible, i.e., $\nabla \cdot \boldsymbol{u} = 0$ and thus the velocity can be obtained from the vorticity by using the Biot-Savart operator. The term on the right hand side is the volume penalization term, which is responsible for imposing the boundary conditions[18,19] and which is absent in the periodic case. The mask function χ is 1 outside the flow-domain, where no-slip walls are imposed and 0 inside the flow, where the Navier-Stokes equations are recovered. The permeability η is chosen sufficiently small for given ν in order to ensure the convergence of the volume penalization method.[19]

The turbulence is kept statistically stationary by a random isotropic stirring. In three-dimensional turbulence, the choice of the forcing scale is trivial in the sense that the only conserved quantity is energy (in the absence of viscosity and considering non-helical flows), which will be transferred to small scales. In general, therefore, if an external forcing is applied, it is applied to the largest scales of the domain in order to observe the largest possible range of interacting scales. In two-dimensional turbulence, however, two quantities are conserved by the nonlinear interaction and these quantities cascade in opposite directions. The energy cascades from the forcing scale to larger scales and the enstrophy to smaller scales. In analogy with three-dimensional turbulence, we will here inject energy in the large scales (in wavenumber $k = 8$ in the present study). A study of the Lagrangian dynamics of wall-bounded turbulence forced at small scales is by itself also interesting, but this will not be attempted in the present study. The inverse cascade of energy will lead to a pile-up of energy at the large scales. To avoid this, we added a Rayleigh friction term to the above equation. In principle, in the wall-bounded geometry, we do not need a friction to avoid a pile up of energy, since the walls act as an enstrophy source and thereby as an energy sink. However, in order to perform a comparison between the two geometries to assess the influence of walls on the statistics, we used the friction in both geometries. We also performed simulations in the wall-bounded case without friction and these results will be presented at the end of the results section. Here and in the following, we will group both energy-injection and Rayleigh friction into the external forcing term

$$\nabla \times \boldsymbol{F} = F_r - \alpha \psi, \qquad (2)$$

with F_r a random forcing, ψ the streamfunction such that $\nabla^2 \psi = \omega$ and α a parameter, taken unity for each simulation. For reasons of numerical stability, the energy injection is time-correlated according to a Markov chain process introduced by Ref. 20 and used in Ref. 21. The forcing term F_r is constructed in physical space using a linear combination of cosine functions. The forcing is limited to wavenumber $k_f = 8$, is isotropic, and its phase is random. In both cases, the time-correlation of the forcing term is smaller than the viscous time-scale, which is the smallest relevant time-scale for the turbulent flow. Particular care was given to the forcing to avoid the injection of angular momentum in the flow. This could lead to the appearance of a large scale structure, completely due to the forcing which would influence the statistics. In order not to inject energy into the solid domain, the forcing term is multiplied by a mask function which smoothly varies from one to zero in the vicinity of the wall. An instantaneous plot of the force F_r is shown in Fig. 1. Since the phase rapidly changes in a random way, the observed structure is not imposed on the flow, but the forcing only determines the scale at which the energy is injected.

The numerical scheme is based on a classical pseudo-spectral method with a resolution of $N = 512^2$ gridpoints and a semi-implicit time integration with $\Delta t = 1 \times 10^{-4}$.[17,19] The Lagrangian quantities are calculated by interpolating the Eulerian quantities and integrated in time using a second order Runge-Kutta scheme. The Lagrangian acceleration is computed as the sum of the pressure gradient, viscous diffusion, and external forcing

$$\begin{aligned} \boldsymbol{a}_L &\equiv \frac{\partial \boldsymbol{u}}{\partial t} + \boldsymbol{u} \cdot \nabla \boldsymbol{u} \\ &= -\nabla p + \nu \nabla^2 \boldsymbol{u} + \boldsymbol{F}. \end{aligned} \qquad (3)$$

We compute the Lagrangian statistics averaged over 10^4 trajectories for each geometry. The viscosity is $\nu = 5 \cdot 10^{-4}$ and the permeability is $\eta = 10^{-4}$. During the statistically stationarity state, the enstrophy fluctuates around a mean value $Z_p = \frac{1}{2}\langle \omega^2 \rangle_x = 136.3$ for the periodic geometry $(.)_p$ and $Z_c = 230$ for the confined geometry $(.)_c$. $\langle . \rangle_x$ denotes the spatial average over the computational domain. The eddy turnover-time is $T_{ep} = 1/\sqrt{2Z_p} = 0.06$ and $T_{ec} = 0.05$, and the Taylor microscale is $\lambda_p = \sqrt{E/Z} = 0.179$, where $E_p = \frac{1}{2}\langle \boldsymbol{u}^2 \rangle_x = 4.39$ is the kinetic energy and $\lambda_c = 0.15$ with $E_c = 4.8$. For the periodic geometry, the Reynolds number is $Re_p = S\sqrt{E}/\nu = 2.6 \times 10^4$, where $S = 2\pi$ corresponds to the domain size. For the circular geometry, the mean

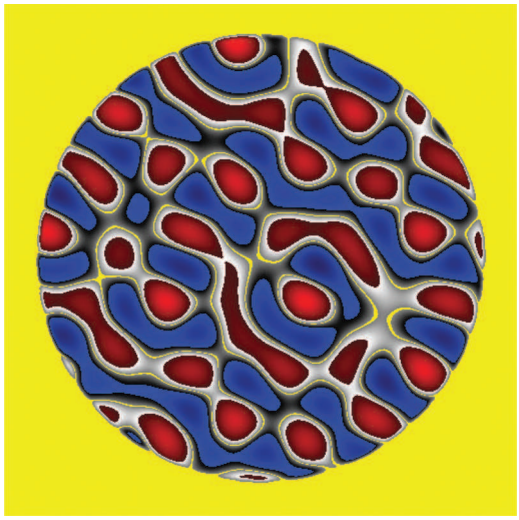

FIG. 1. (Color online) Instantaneous plot of the forcing term F_r using the same color table as in Fig. 3.

Reynolds number is $Re_c = 2R\sqrt{E}/\nu = 2.4 \times 10^4$, where $R = 2.8$ is the radius of the circle. The Reynolds number based on the Taylor microscale is for the periodic geometry $R_{\lambda p} = \lambda\sqrt{E}/\nu = 751$ and for the circular geometry $R_{\lambda c} = 633$. These physical parameters for both configurations are similar, so the flows in the different geometries are comparable with respect to these quantities. Details on the Eulerian properties of a similar decaying flow can be found in Ref. 19. The integration is done for $5 \cdot 10^5$ timesteps which corresponds to $800T_{ep}$ and $1000T_{ec}$.

III. RESULTS

A. Comparison of Lagrangian statistics in periodic and wall-bounded domains

In this section, we present results of Lagrangian quantities in the statistically stationary state, i.e., the energy and enstrophy are fluctuating around a constant value as shown in Fig. 2. For the circular geometry, the mean energy is slightly stronger than for the periodic geometry, and the enstrophy exhibits stronger fluctuations.

In Fig. 3 (top), the visualization of vorticity fields shows for both geometries the presence of coherent structures which have approximately the same maximum length scale in the periodic case and in the center of the confined case. Moreover, in the circular geometry, the no-slip boundary conditions generate a thin turbulent boundary layer which destabilizes and detaches, ejecting coherent vortices into the bulk-flow, which can explain the stronger fluctuation of the enstrophy observed in Fig. 2. For each geometry, one typical particle trajectory is plotted and is colored by the amplitude of the Lagrangian acceleration in Fig. 3 (bottom).

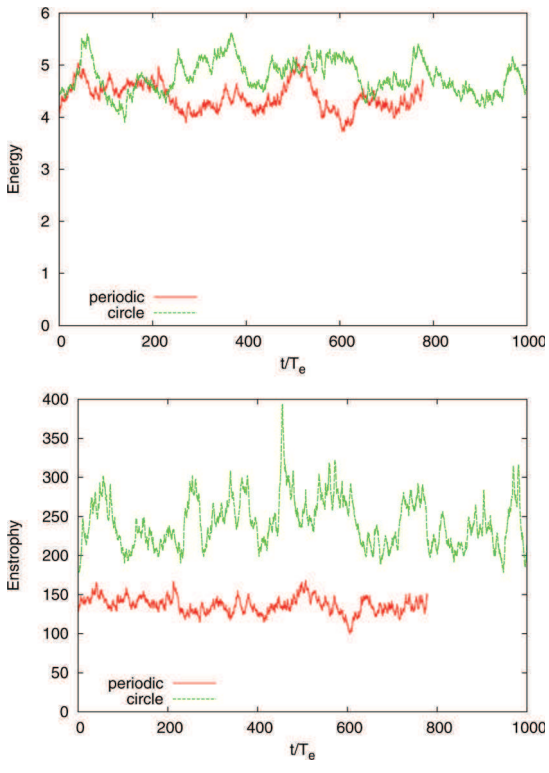

FIG. 2. (Color online) Top: time evolution of the energy $E(t)$ for periodic and circular geometry. Bottom: time evolution of the enstrophy $Z(t)$ for periodic and circular geometry.

The PDFs of the Eulerian vorticity, shown in Fig. 4, are symmetric and exhibit heavier tails in the circular domain due to the intermittent creation of vorticity at the walls.

A first statistical measure which can quantify the influence of confinement is the single particle dispersion. This quantity yields some information on the correlation time of the turbulence and on the time at which the confinement starts to limit the distance between the current and the initial positions. The studied quantity is the mean of the square distance between the current and the initial position

$$\langle (X(t) - X(0))^2 \rangle_n, \tag{4}$$

which is shown in Fig. 5. Here, $\langle \cdot \rangle_n$ corresponds to the ensemble average (average over the particles) and X denotes the x-coordinate of the tracer. The dispersion follows a t^2 behavior for short times which is characteristic for a ballistic regime. For long times, we observe a Brownian regime ($\propto t$ slope) in the periodic case which is consistent with theory[22] and a plateau in the confined case. The latter is due to the limited size of the domain. We note that the dispersion does not present a Brownian regime in the circle. It is expected that if the domain size would be larger while keeping the integral length scale of the turbulence unchanged, a Brownian regime would be recovered for intermediate times. Note that almost identical results are obtained for the y-coordinate Y, which gives evidence for sufficient statistical sampling.

The PDFs of the Lagrangian velocity, shown in Fig. 6 (top) and in Fig. 7 (top), show a close to Gaussian behavior except around zero for the circular geometry where a small cusp appears. This is explained by the no-slip condition at the wall which induces an enhanced probability to find particles with a velocity close to zero, leading to a higher probability of zero velocity. Moreover, these PDFs are very similar to the ones obtained in decaying turbulence.[16] In Fig. 6 (bottom), the PDFs of the time-averaged Lagrangian velocity increments, defined by

$$\Delta u_L(\tau) = \langle u_L(t+\tau) - u_L(t) \rangle, \tag{5}$$

are shown, $\langle \cdot \rangle$ is the ensemble average, averaged in time. The PDFs are symmetric for both cases. For small τ, the PDFs of the Lagrangian velocity increments tend to the ones of the Lagrangian acceleration, shown in Fig. 6 (bottom), and they present similar extreme values when the Lagrangian acceleration is normalized, see Fig. 7 (center). For large τ, the PDFs of the Lagrangian velocity increments tend to the PDF of the Lagrangian velocity. The difference between the two configurations is highlighted in Fig. 7 (center) where the PDFs of the Lagrangian acceleration for both cases are superposed. For both cases, the tails of the PDFs are close to exponential. The PDFs almost collapse, apart from the tails, corresponding to rare events with a magnitude larger than 10 times the standard deviation. The PDFs are normalized so that all information on the variance of the acceleration is removed from the PDFs. These are reported in Table I. The standard deviation of the Lagrangian acceleration is $\sigma_{a_{Lp}} = 24$ for the periodic geometry and $\sigma_{a_{Lc}} = 47$ for the

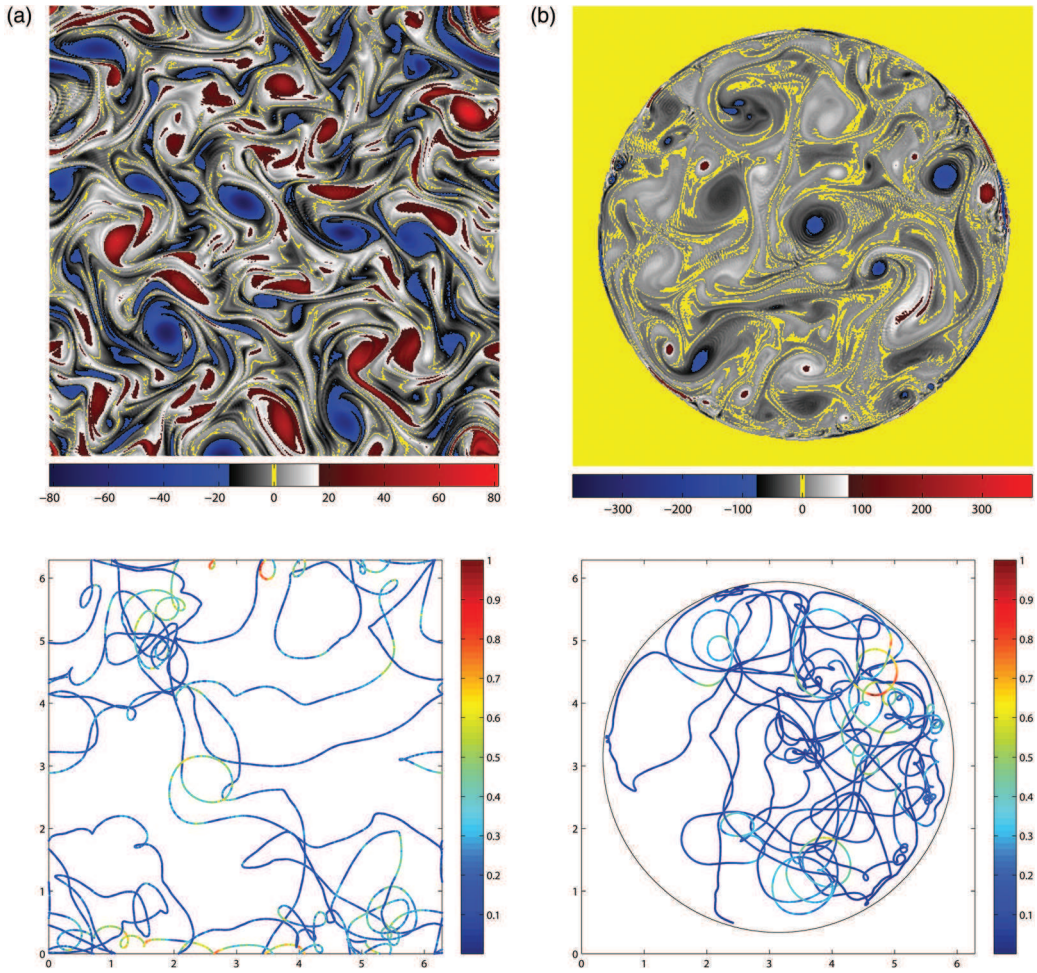

FIG. 3. (Color online) Top: snapshots of vorticity fields at $t = 50$. Bottom: one trajectory colored by the Lagrangian acceleration amplitude divided by its maximum value (periodic: $max = 115$, circle: $max = 434$). a and b correspond to the periodic and circular domains, respectively.

confined case. The standard deviation of the Lagrangian acceleration is hence 2 times stronger in the circular geometry while the mean values of the energy are similar for both geometries. The mean value of the enstrophy is not equal in the two flows and we will come back to this issue later. The resulting difference in the variance of the Lagrangian acceleration is illustrated by plotting non normalized PDFs in Fig. 7 (bottom).

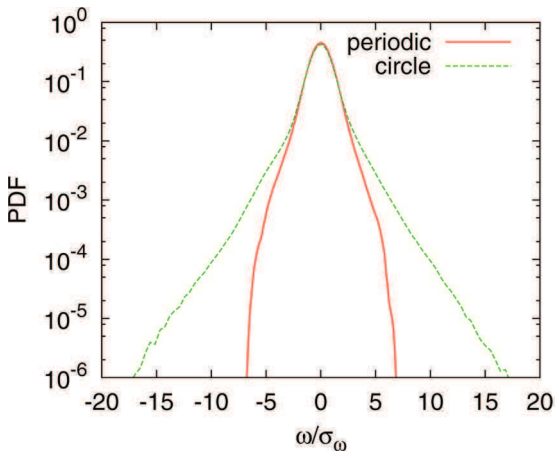

FIG. 4. (Color online) PDFs of the Eulerian vorticity normalized by their standard deviation for the periodic and circular domain.

We note that in Table I also all the different contributions to the acceleration are shown. This analysis is inspired by the work of Ref. 23. It is observed that the variance of the pressure gradient is approximately identical to the variance of the acceleration. In comparison, the viscous term is very small.

The flatness of the Lagrangian velocity increments is shown in Fig. 8. At small τ, the flatness of the components tends to a value of 20 for both geometries. At larger τ, a steep descent is observed, approaching the Gaussian value 3 rapidly, which corresponds to the flatness of the Lagrangian velocity. Also shown is the flatness of the norm of the velocity increments. This flatness tends to 2 for large τ. This is a logical consequence of the Gaussianity of the velocity. If a quantity is Gaussian distributed, then its norm is χ-distributed. The flatness of a D-dimensional χ-distribution is $(D+2)/D$, so 2 for two dimensions.

The autocorrelation functions of the Lagrangian velocity and acceleration are plotted in Figs. 9 and 10. Qualitatively, the correlations are similar to autocorrelations obtained in three-dimensional homogeneous isotropic turbulence.[5] In the inset of Fig. 9 (top), we fit the autocorrelation of the Lagrangian velocity to an exponential function, $\exp(-t/T_L)$, where T_L is a Lagrangian time scale which is equal to 0.18 and 0.11 for periodic and circular geometries, respectively. The

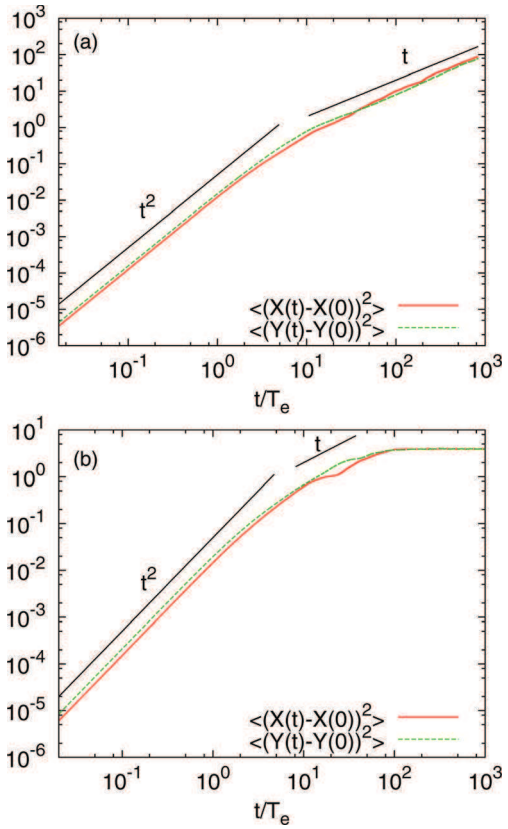

FIG. 5. (Color online) Single particle dispersion for periodic and circular geometry. a and b correspond to the periodic and circular domains, respectively.

difference between the two configurations is that in the circle the autocorrelation of the Lagrangian velocity exhibits at short increment time negative values. This might be related to the more dominant spiraling motion of the trajectories in the wall-bounded flow as observed in Figure 3.

The autocorrelation of the Lagrangian acceleration decays faster than the one of the Lagrangian velocity and is again very similar for both geometries. For large values of τ, the autocorrelation of the Lagrangian acceleration tends to zero and becomes completely uncorrelated. Note that a small negative bias at long times has been corrected, similar to what was done in the work by Yeung and Pope,[3] and attributed there to the statistical fluctuations of the considered quantity. As observed in, e.g., Ref. 24, the time-correlation of the norm of the acceleration is an order of magnitude larger than the time-correlation of the components. The explanation is the dominating circular motion of fluid particles. Indeed, during a circular motion, the norm of the acceleration is constant, whereas its components change constantly.

Fig. 11 shows spectra of the Lagrangian velocity as a function of frequency w. In both spectra, no clear inertial zone can be identified. If arguments à la Kolmogorov are applied to Lagrangian spectra, the scaling of the spectrum in 3D would be proportional to w^{-2}.[25] The same would also be the case in the inverse cascade regime in two-dimensions. Here, we consider the forward enstrophy cascade and it is not known which scaling should be expected. For comparison, we indicate in the figures the w^{-2} power law. However,

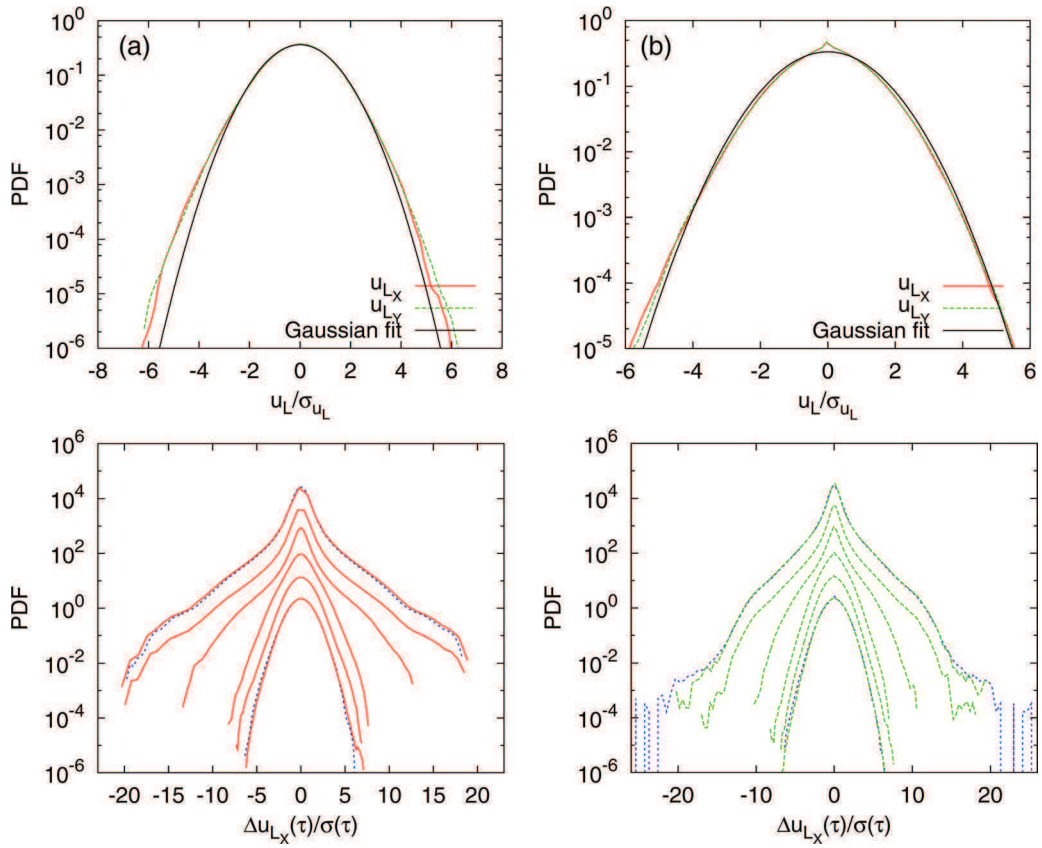

FIG. 6. (Color online) Top: PDFs of normalized Lagrangian velocities u_L/σ_{u_L}, where $\sigma_{u_L} = \langle u_L^2 \rangle^{1/2}$. Bottom: PDFs of normalized Lagrangian velocity increments $\Delta u_L(\tau)/\sigma(\tau)$, where $\sigma(\tau) = \langle (\Delta u_L(\tau))^2 \rangle^{1/2}$. a and b correspond to the periodic and circular domains, respectively.

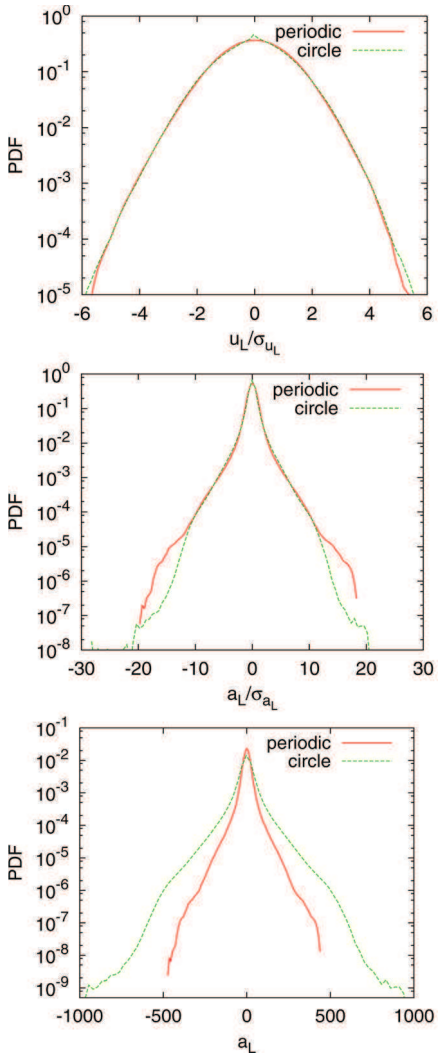

FIG. 7. (Color online) Top: PDFs of normalized Lagrangian velocities u_L/σ_{u_L}. Center: PDFs of the normalized Lagrangian acceleration a_L/σ_{a_L}. Bottom: PDFs of the non-normalized Lagrangian acceleration.

if a power-law is to be observed, it would be closer to w^{-1}, in particular in the circular geometry. The Lagrangian velocity spectrum for the periodic geometry presents a plateau for lower frequencies, $w < 20$, while for the circular geometry, the Lagrangian velocity spectrum exhibits a bump.

TABLE I. Standard deviation of the Lagrangian quantities, showing only the x-component. The y-components, which should by symmetry-considerations converge to the same value, are all within 1% of the x-values and are thus omitted. u_{L_X} corresponds to the Lagrangian velocity, a_{L_X} is the Lagrangian acceleration, $a_{\nabla p_X}$ is the pressure gradient, $a_{\nu\nabla^2 u_{LX}}$ is the viscous term, a_{F_X} is the forcing term, $a_{u_L\cdot\nabla u_{LX}}$ is the advective term and $a_{\frac{\partial u_L}{\partial t}X}$ is the time derivative of the velocity.

	Periodic	Circle
u_{L_X}	1.891	2.461
a_{L_X}	23.93	46.53
$a_{\nabla p_X}$	21.95	44.92
$a_{\nu\nabla^2 u_{LX}}$	0.11	0.38
a_{F_X}	9.77	12.85
$a_{u_L\cdot\nabla u_{LX}}$	25.59	52.15
$a_{\frac{\partial u_L}{\partial t}X}$	16.33	29.61

B. Is the influence of the walls localized in a small region?

In this subsection, we will investigate if the influence of the walls is localized in the near-wall region or if it is affecting the complete domain. Indeed, in the foregoing analysis, the quantities were averaged over all trajectories, sampling thereby the complete domain. In this section, we will focus separately on the near-wall region and the center-region of the circular domain. We proceed as follows: we choose an arbitrary radius $r_c \leq R$ and separate the statistics into two parts, inside and outside the selected radius. A single trajectory can thus contribute to both regions. The flatness of the conditional Lagrangian acceleration $a_{L_{r>r_c}}(t)$ is defined as

$$F^{\mathrm{EXT}}(a_L, r_c) = \frac{\langle a_L(r)^4 \rangle_{r>r_c}}{\langle a_L(r)^2 \rangle^2_{r>r_c}}, \tag{6}$$

where $\langle\cdot\rangle_{r>rc}$ denotes the ensemble average, averaged in time, for the particles confined to the annular subdomain defined by the radius $r > r_c$. For $r_c/R = 0$, we thus consider the whole domain, and approaching $r_c/R = 1$, the subdomain is confined to the near wall region. Analogously, we define the flatness of the internal sub-domain

$$F^{\mathrm{INT}}(a_L, r_c) = \frac{\langle a_L(r)^4 \rangle_{r<r_c}}{\langle a_L(r)^2 \rangle^2_{r<r_c}}. \tag{7}$$

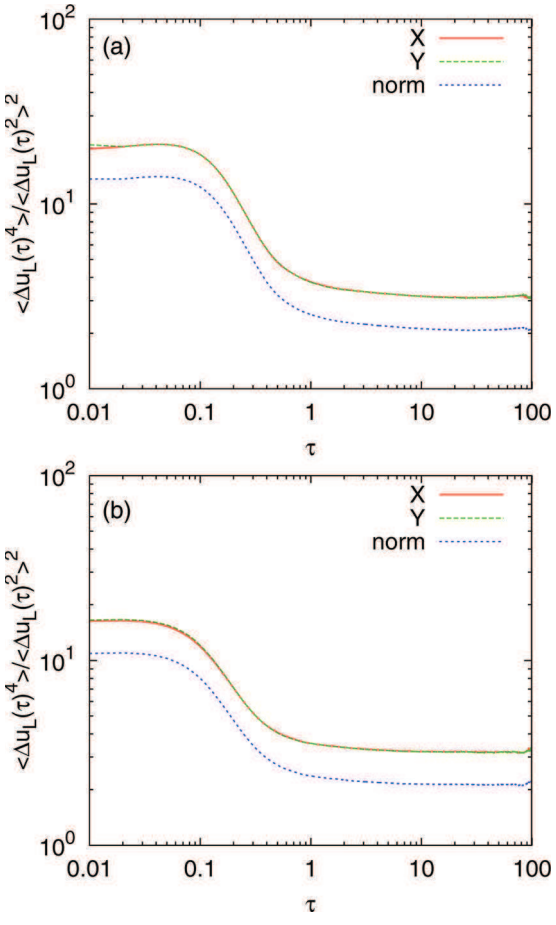

FIG. 8. (Color online) Flatness as function of increments τ for periodic and circular geometry. a and b correspond to the periodic and circular domains, respectively.

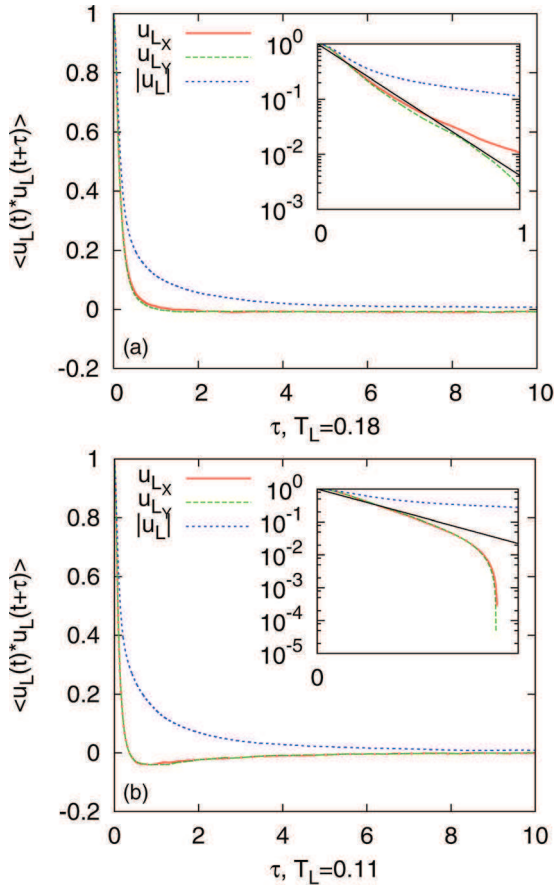

FIG. 9. (Color online) Lagrangian velocity autocorrelation for periodic and circular geometry. a and b correspond to the periodic and circular domains, respectively.

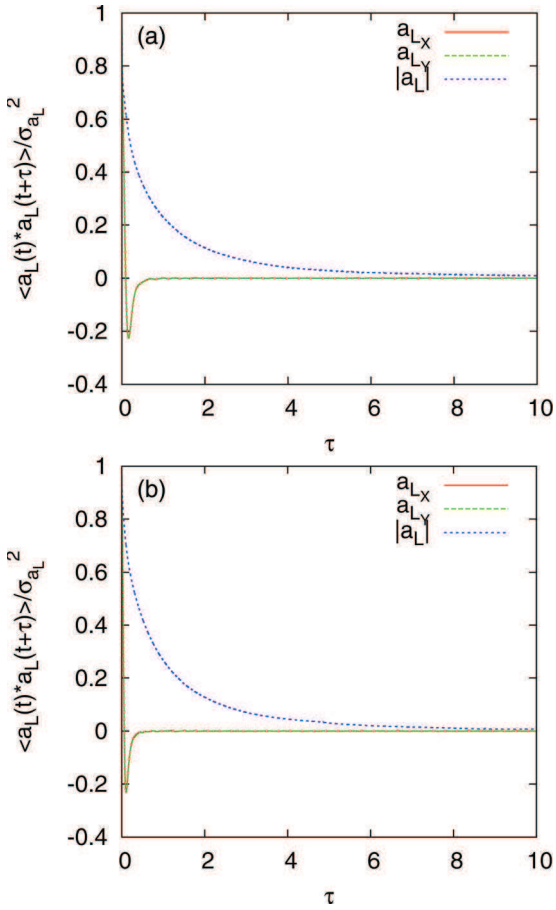

FIG. 10. (Color online) Lagrangian acceleration autocorrelation for periodic and circular geometry. a and b correspond to the periodic and circular domains, respectively.

This quantity thus gives the flatness of the Lagrangian-acceleration confined to a circular domain with radius r_c. The conditional flatnesses are plotted in Fig. 12 for the case of the circular geometry. The value in the periodic domain, which due to the flow homogeneity does not depend on r, is also indicated.

For a radius $r_c/R < 0.6$, the flatness F^{EXT} is nearly constant with a value of about 16. Then, for $r_c/R > 0.6$, the conditional flatness strongly increases. Since the flatness is constant for $r_c/R < 0.6$, it is tempting to state that no significant influence of the wall can be found for the acceleration in the center of the domain. However, if we compare with the value in the periodic domain, we see that the flatness is significantly changed by the presence of walls. This non-negligible influence becomes constant in the center of the domain but does not vanish. In the region $r_c/R > 0.6$, the influence of the walls becomes increasingly stronger. Note that for the largest radius, the value of the conditional flatness may not be converged since the domains become too small and the statistical sampling is no longer sufficient.

These results enable us to reassess the conditional flatness in Ref. 16. We do not observe the sharp transition of the flatness for $r_c/R > 0.3$ as was observed in Ref. 16. Indeed closer inspection of the results in Ref. 16 showed that the sharp increase was caused by a problem of statistical convergence and an inhomogeous initial distribution of the particles. In the present study, the particles are spread initially homogeneously, and the statistically stationary flow allows to obtain better converged statistics. A further difficulty with Ref. 16 was that during the computation, the enstrophy strongly decayed, leading to statistics averaged over strongly varying flow-conditions. The stationarization used allows to compensate for the energy decay but not for this enstrophy decay. However, also in the present study, we observe a strong increase of the conditional flatness for $r_c/R > 0.7$

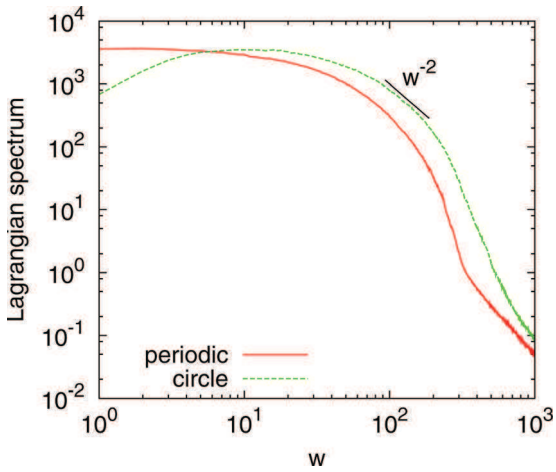

FIG. 11. (Color online) Lagrangian velocity spectra for periodic and circular geometry.

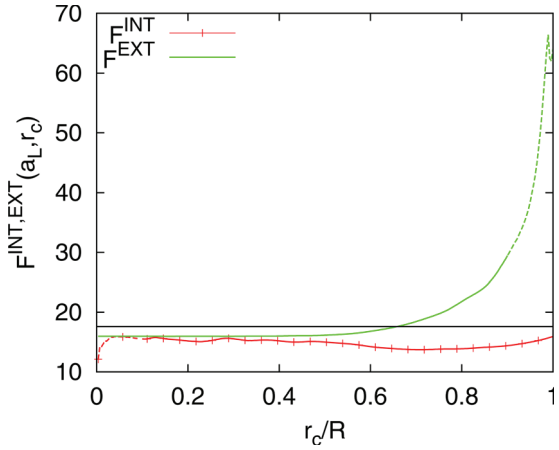

FIG. 12. (Color online) Conditional statistics as a function of radius r_c/R for the circular geometry. The lines for F^{EXT} and F^{INT} are shown with a solid line where we trust the statistics and by dashed line in the remaining bits.

which indicates the presence of a Lagrangian boundary layer, be it smaller and less sharp than the one found in Ref. 16.

The PDFs corresponding to these subdomains are shown in Figure 13 which confirms that the extreme values of the Lagrangian acceleration appear for regions close to the wall. For completeness, we also show in Figure 14, the enstrophy as a function of the radius r. It is observed that the value of the enstrophy increases rapidly in the vicinity of the wall. We will focus on the influence of the value of the enstrophy on the Lagrangian statistics in the next paragraph.

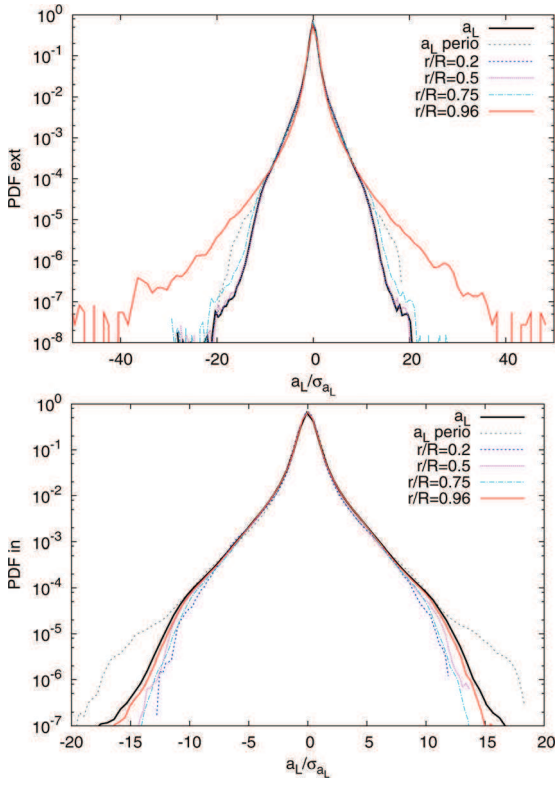

FIG. 13. (Color online) PDFs of the acceleration in the subdomain defined by $r > r_c$ (top) and $r < r_c$ (bottom) for the circular geometry, compared to the PDF in the periodic domain.

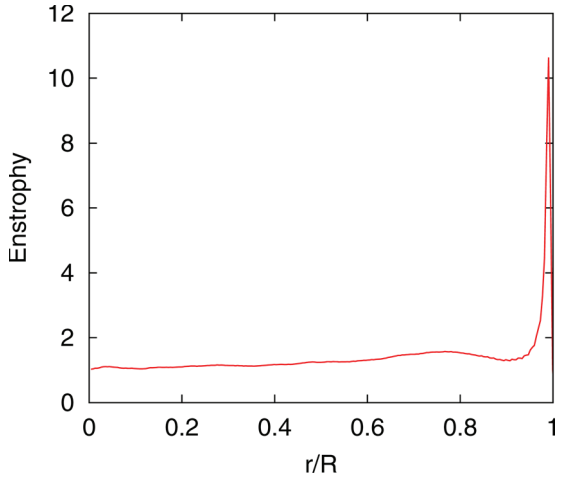

FIG. 14. (Color online) Enstrophy as function of the radius in the circular geometry.

C. The influence of the level of enstrophy on the Lagrangian acceleration

Comparing the PDFs in Figure 7, we observe that the shape of the PDF of the Lagrangian acceleration is very similar for the two geometries, but that the standard deviation changes considerably. In both geometries, the kinetic energy is maintained on the same level, but this implies a higher level of enstrophy in the circular geometry, as is observed in Figure 2. The reason for this is that the solid

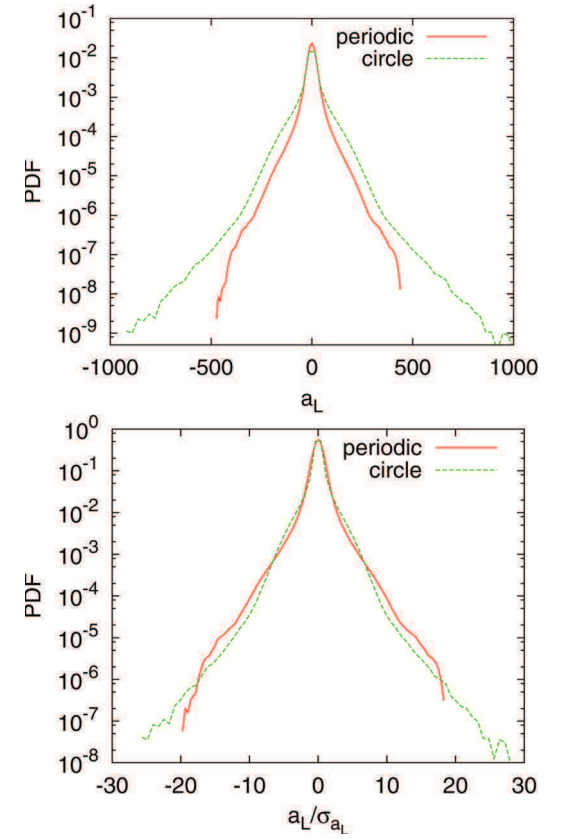

FIG. 15. (Color online) The PDFs of the Lagrangian acceleration for the case in which both the enstrophy and the energy are maintained at the same level in both geometries. Top: normalized PDFs, bottom: non-normalized PDFs.

boundaries in the circular domain act as an energy sink by producing enstrophy. In order to obtain the same level of energy, the forcing strength has to be increased in the circular domain. The resulting flow has a higher level of enstrophy at equal energy. A question which can be asked at this point is how the flow statistics would change if both the energy and the enstrophy level are the same in both flows. We managed to create such a flow by removing the Rayleigh friction in the circular domain and adapting the forcing strength. Both the energy and enstrophy level are comparable in the resulting flow, with some strong enstrophy fluctuations around the mean value in the circular geometry. For this flow, we show the PDFs of the Lagrangian acceleration in Figure 15. The striking difference with Figure 7 is the approximate collapse of the non-normalized PDFs, while the standard deviation of the Lagrangian acceleration is 1.5 times stronger in the circular geometry. This is an indication that the standard deviation of the Lagrangian acceleration is intimately related to the level of enstrophy of the flow. Indeed the presence of stronger enstrophy fluctuations, due to intermittent vorticity generation at the wall, probably explains the stronger standard deviation in the circular domain, although the mean values of enstrophy are similar for both geometries. Moreover, the normalized PDFs do not collapse as well as those in Figure 7. Clearly, the presence of a large-scale friction influences the shape of the PDF of the Lagrangian acceleration, since we need more enstrophy to obtain similar energy for both cases.

The present observations infer, therefore, that the main influence of the walls on the PDFs of the Lagrangian acceleration is the enhancement of the level of enstrophy, which leads to a higher standard deviation of the Lagrangian acceleration.

IV. CONCLUSION

In this study, we showed the influence of no-slip conditions on the Lagrangian statistics of passive tracers. For that, we performed direct numerical simulations of two-dimensional statistically stationary incompressible turbulent flow in periodic and circular domains, for the latter with no-slip boundary conditions. The influence of the wall was assessed by analyzing the Lagrangian statistics. As found in Ref. 16, the presence of solid boundaries influences in particular the behavior of the Lagrangian acceleration. When considering subdomains including or not the near-wall region, we observe that the influence of the walls becomes approximately constant in a central region, which allows to define a Lagrangian boundary layer, be it less pronounced than in Ref. 16. However, comparing this center region with fully periodic flows, a difference remains. This difference is traced back to the enstrophy which is produced at the walls and diffuses into the domain. In the periodic domain, no enstrophy production exists, except for the homogeneous force term. The influence of walls is thus not confined to a small near-wall region but influences the entire domain. As in Ref. 16, we can conclude that, since a large number of experiments on Lagrangian tracers are carried out in wall-bounded geometry, the universality of these experimental results can be questioned. However, it is possible that the effects in three-dimensional turbulence are decaying faster as a function of the distance to the wall since enstrophy is no conserved quantity in three dimensions. In order to answer this question, a three dimensional extension of the present study constitutes an important perspective.

ACKNOWLEDGMENTS

The authors thank G. Keetels for discussions about computing the forcing term.

[1]S. B. Pope, *Turbulent Flows* (Cambridge University Press, 2000).
[2]X. Shen and Z. Warhaft, "The anisotropy of the small scale structure in high Reynolds number ($R_\lambda \sim 1000$) turbulent shear flow," Phys. Fluids **12**, 2976 (2000).
[3]P. K. Yeung and S. B. Pope, "Lagrangian statistics from direct numerical simulations of isotropic turbulence," J. Fluid Mech. **207**, 531 (1989).
[4]A. La Porta, G. A. Voth, A. M. Crawford, J. Alexander, and E. Bodenschatz, "Fluid particle accelerations in fully developed turbulence," Nature **409**, 1017 (2001).
[5]N. Mordant, E. Lévêque, and J.-F. Pinton, "Experimental and numerical study of the Lagrangian dynamics of high Reynolds turbulence," New J. Phys. **6**, 116 (2004).
[6]F. Toschi and E. Bodenschatz, "Lagrangian properties of particles in turbulence," Annu. Rev. Fluid Mech. **41**, 375 (2009).
[7]P. K. Yeung, "Lagrangian investigations of turbulence," Annu. Rev. Fluid Mech. **34**, 115 (2002).
[8]M. Wilczek, O. Kamps, and R. Friedrich, "Lagrangian investigation of two-dimensional decaying turbulence," Physica D **237**, 2090 (2008).
[9]O. Kamps and R. Friedrich, "Lagrangian statistics in forced two-dimensional turbulence," Phys. Rev. E **78**, 036321 (2008).
[10]W. J. T. Bos, B. Kadoch, S. Neffaa, and K. Schneider, "Lagrangian intermittency in drift wave turbulence," Physica D **239**, 1269 (2010).
[11]B. Kadoch, D. del-Castillo-Negrete, W. J. T. Bos, and K. Schneider, "Lagrangian statistics and flow topology in forced two-dimensional turbulence," Phys. Rev. E **83**, 036314 (2011).
[12]S. Ayyalasomayajula, A. Gylfason, L. R. Collins, E. Bodenschatz, and Z. Warhaft, "Lagrangian measurements of inertial particle accelerations in grid generated wind tunnel turbulence," Phys. Rev. Lett. **97**, 144507 (2006).
[13]N. Mordant, P. Metz, O. Michel, and J.-F. Pinton, "Measurements of Lagrangian velocity in fully developed turbulence," Phys. Rev. Lett. **87**, 214501 (2001).
[14]N. T. H. Ouellette, H. Xu, M. Bourgoin, and E. Bodenschatz, "Small-scale anisotropy in Lagrangian turbulence," New J. Phys. **8**, 102 (2006).
[15]N. M. Qureshi, U. Arrieta, C. Baudet, A. Cartellier, Y. Gagne, and M. Bourgoin, "Acceleration statistics of inertial particles in turbulent flow," Eur. Phys. J. B **66**, 531 (2008).
[16]B. Kadoch, W. J. T. Bos, and K. Schneider, "Extreme Lagrangian acceleration in confined turbulent flow," Phys. Rev. Lett. **100**, 184503 (2008).
[17]K. Schneider and M. Farge, "Decaying two-dimensional turbulence in a circular container," Phys. Rev. Lett. **95**, 244502 (2005).
[18]P. Angot, C.-H. Bruneau, and P. Fabrie, "A penalisation method to take into account obstacles in viscous flows," Numer. Math. **81**, 497 (1999).
[19]K. Schneider, "Numerical simulation of the transient flow behaviour in chemical reactors using a penalisation method," Comput. Fluids **34**, 1223 (2005).
[20]D. Lilly, "Numerical simulation of two-dimensional turbulence," Phys. Fluids **12**(Suppl. II), 233 (1969).
[21]G. Keetels, "Fourier spectral computation of geometrically confined two-dimensional flows," Ph.D. thesis (T.U. Eindhoven, 2008).
[22]G. I. Taylor, "Diffusion by continuous movements," Proc. London Math. Soc. **20**, 196 (1921).
[23]A. Tsinober, P. Vedula, and P. K. Yeung, "Random Taylor hypothesis and the behavior of local and convective accelerations in isotropic turbulence," Phys. Fluids **13**, 1974 (2001).
[24]N. Mordant, J. Delour, E. Lévêque, A. Arneodo, and J.-F. Pinton, "Long time correlations in Lagrangian dynamics: A key to intermittency in turbulence," Phys. Rev. Lett. **89**, 254502 (2002).
[25]H. Tennekes and J. L. Lumley, *A First Course in Turbulence* (The MIT, 1972) mitpress.mit.edu/0262200198.